ARM Total Sky Imager: Monte Carlo Simulations

E. I. Kassianov, C. N. Long, and M. Ovtchinnikov
Pacific Northwest National Laboratory
Richland, Washington

Introduction

The Atmospheric Radiation Measurement (ARM) Program is currently operating Total Sky Imagers (TSI) at various sites (see http://www.arm.gov). These ground-based instruments have a *hemispherical* field-of view (FOV) and provide time series of fractional sky cover $N_{hemisph}$. However, only the nadir-view cloud fraction N_{nadir} is directly applicable for radiation calculations and climate studies. Therefore, there is an essential need to establish the relationship between N_{nadir} and $N_{hemisph}$. In this paper, we (1) estimate sensitivity of these two bulk temporal statistics to the cloud evolution and (2) demonstrate how accurately N_{nadir} can be estimated from TSI (hemispherical) observations. We simulate TSI measurements by using the Monte Carlo method and the results of large eddy simulation (LES) mode.

Nadir View Cloud Fraction and Fractional Sky Cover

Let us consider a TSI located at the surface. We assume that this instrument has a FOV with the cone zenith angle *2a*. Also we assume that a single cloud layer with cloud base height, *Hb*, located above this TSI and cloud base height does not change significantly within the FOV. Therefore, projection of the FOV onto the horizontal surface at height *Hb* is a circle with radius $R(\alpha)$. The radius $R(\alpha)$ is connected to the cone zenith angle *a* and *Hb as* $R(\alpha) = Hb\ tg\alpha$.

For a given FOV, we compare (1) the nadir-view cloud fraction $N_{nadir}\ (\alpha)$ and (2) the fractional sky cover $N_{hemisph}\ (\alpha)$.

The nadir-view cloud fraction $N_{nadir}(\alpha)$ can be defined as a ratio:

$$N_{nadir}(\alpha) = \frac{S_{cld,\,nadir}(\alpha)}{S_{nadir}(\alpha)} \tag{1}$$

where $S_{cld,\,nadir}(\alpha)$ is horizontal cloud area as viewed from the *nadir* (within the circle with radius $R[\alpha]$); $S_{nadir}(\alpha) = \pi R^2(\alpha)$ is the area of this circle. The dimensions of $S_{cld,\,nadir}(\alpha)$ and $S_{nadir}(\alpha)$ are km^2.

The fractional sky cover $N_{hemisph}(\alpha)$ can be defined as a ratio:

$$N_{hemisph}(\alpha) = \frac{S_{cld,\,hemisph}(\alpha)}{S_{hemisph}(\alpha)} \tag{2}$$

where $S_{hemisph}(\alpha)$ is the observed solid angle with cone zenith angle 2α (as viewed by a surface observer):

$$S_{hemisph}(\alpha) = \int_0^{2\pi} d\varphi \int_0^{\alpha} \sin\theta \, d\theta = 2\pi(1-\cos\alpha) \tag{3}$$

and $S_{cld,\ hemisph}(\alpha)$ is the fraction of this solid angle filled by clouds. In contrast to $S_{cld,\ nadir}(\alpha)$ and $S_{nadir}(\alpha)$, the dimensions of $S_{cld,\ hemisph}(\alpha)$ and $S_{hemisph}(\alpha)$ are the steradian.

The next simple example illustrates the differences between N_{nadir} and $N_{hemisph}$. Let us consider a single cloud located within the FOV (within the circle with radius $R(\alpha^*)$, $\alpha^* = 80$). This cloud has a shape of a cylinder with variable radius R_{cld}. The cloud thickness is an infinitesimal quantity, therefore the cylinder can be considered as a circle with variable radius R_{cld}. For simplicity, we assume that the center of these two circle (with radius $R(\alpha^*)$ and R_{cld}) are the same, and $R_{cld}(\alpha) = Hb\ tg\alpha$, where $\alpha \le \alpha^*$. From (1) and (2) follows that

$$N_{nadir}(\alpha^*) = \frac{\pi R^2{}_{cld}(\alpha)}{\pi R^2(\alpha^*)} = \frac{(tg\alpha)^2}{(tg\alpha^*)^2} \tag{4}$$

and

$$N_{hemisph}(\alpha^*) = \frac{2\pi(1-\cos\alpha)}{2\pi(1-\cos\alpha^*)} = \frac{1-\cos\alpha}{1-\cos\alpha^*} \tag{5}$$

Figure 1a shows $N_{nadir}(\alpha^*)$ and $N_{hemisph}(\alpha^*)$ as functions of the cone zenith angle α (or cloud size $R_{cld}[\alpha]$). It is seen that $N_{hemisph}(\alpha^*)$ is substantially larger than $N_{nadir}(\alpha^*)$ if a small/intermediate cloud is located in the center of FOV.

It can be easily demonstrated that the opposite ($N_{hemisph}[\alpha^*] < N_{nadir}[\alpha^*]$) is true when a cloud (or its parts) is located near the edge of the FOV. Assume that (1) a cloud has a shape of a washer; (2) centers of the circle and the washer are the same. The washer has a constant outer radius $R(\alpha^*)$ and variable inner radius $R(\alpha)$, where $\alpha \le \alpha^*$; the washer thickness is an infinitesimal quantity. In this case

$$N_{nadir}(\alpha^*) = 1 - \frac{(tg\alpha)^2}{(tg\alpha^*)^2} \tag{6}$$

and

$$N_{hemisph}(\alpha^*) = 1 - \frac{1-\cos\alpha}{1-\cos\alpha^*} \tag{7}$$

Figure 1b demonstrates that $N_{hemisph}(\alpha^*) << N_{nadir}(\alpha^*)$ when the cloud covered area is near the edge of the FOV, i.e., α is large. Note that for any given cloud size, $N_{nadir}(\alpha^*)$ is independent of the cloud position within the circle with radius $R(\alpha^*)$. In contrast, $N_{hemisph}(\alpha^*)$ can be sensitive to the cloud location.

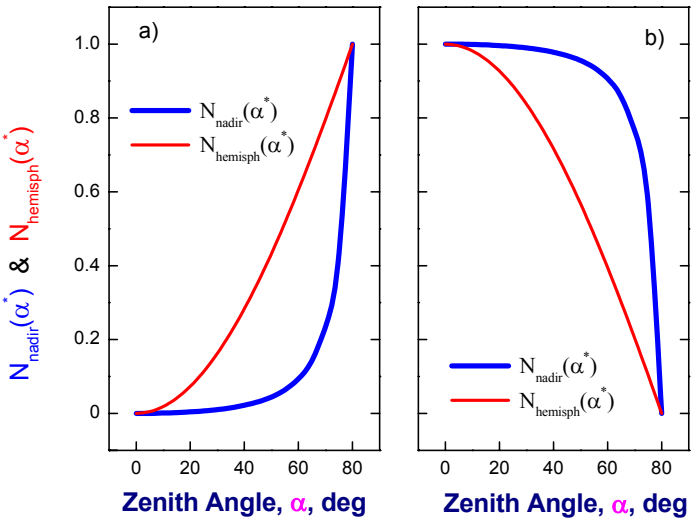

Figure 1. Ratios $N_{nadir}(\alpha^*)$ and $N_{hemisph}(\alpha^*)$ as functions of the cone zenith angle α, which are obtained from (a) Eqs. 4, 5 and (b) Eqs. 6, 7.

Here we considered the simplest case only: (1) a single cloud with no vertical extent, (2) cloud shape was unrealistic, very simple and static, and (3) cloud center does not move. Real cloud fields contain three-dimensional (3D) clouds with irregular and complex geometry. The geometry of individual clouds is time dependent. Cloud fields move across the FOV during observations. Therefore, when real clouds travel across the FOV (in wind direction) the difference between $N_{hemisph}(\alpha^*)$ $N_{nadir}(\alpha^*)$ can change both the magnitude and the sign. As a result, the time-averaged values of $N_{hemisph}(\alpha^*)$ and $N_{nadir}(\alpha^*)$ could be closely related. To verify this assumption, we use a four-dimensional (three spatial and one temporal) cloud field provided by LES model.

Approach

First we estimate sensitivity of $N_{nadir}(\alpha)$ and $N_{hemisph}(\alpha)$ to the cloud evolution. We obtain two sets of four-dimensional cloud fields by using LES simulation data (Figure 2). The first set captures the cloud field motion only. In other words, the Taylor's frozen flow hypothesis is applied. The second set captures both individual clouds evolution and cloud field motion. These two sets are used as input for Monte Carlo simulations of TSI measurements. Monte Carlo results obtained for the second set are considered as reference.

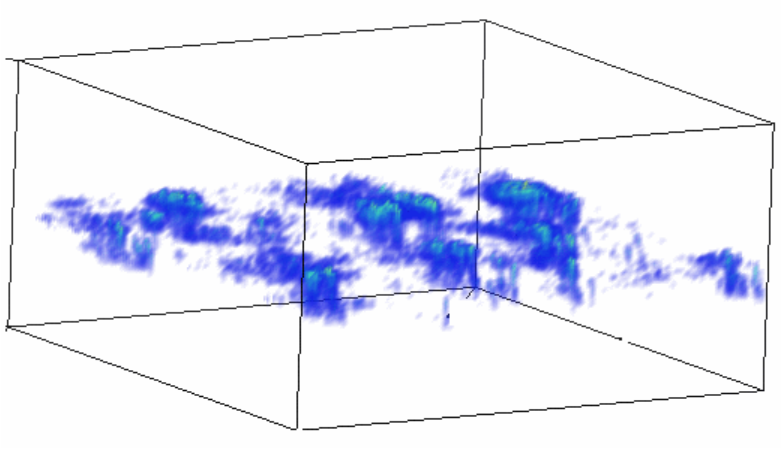

Figure 2. One of the 3D cloud fields generated by LES model.

Temperature and moisture profiles from soundings at the ARM Tropical Western Pacific (TWP) site (Nauru) are used for LES simulation. Simulations are performed for the domain 10 x 10 x 2 km^2 with 0.1 km (horizontal) and 0.033 km (vertical) resolution. The output of this simulation is the temporal sequence of 3D cloud fields with 3-min step. Within 15-min time window the geometry of individual clouds can change significantly (Figure 3), but these geometrical changes have only a slight effect on the domain-averaged cloud fraction $N_{nadir,\ avr}$ (variations of $N_{nadir,\ avr}$ are ~10%). For Monte Carlo simulations we assumed that advection flow (mean wind speed) is 10 m/sec, the cloud fields move in the y-direction (wind direction), and the averaging period (temporal sample size) is 15 min. We perform the Monte Carlo simulations by assuming the periodical boundary conditions.

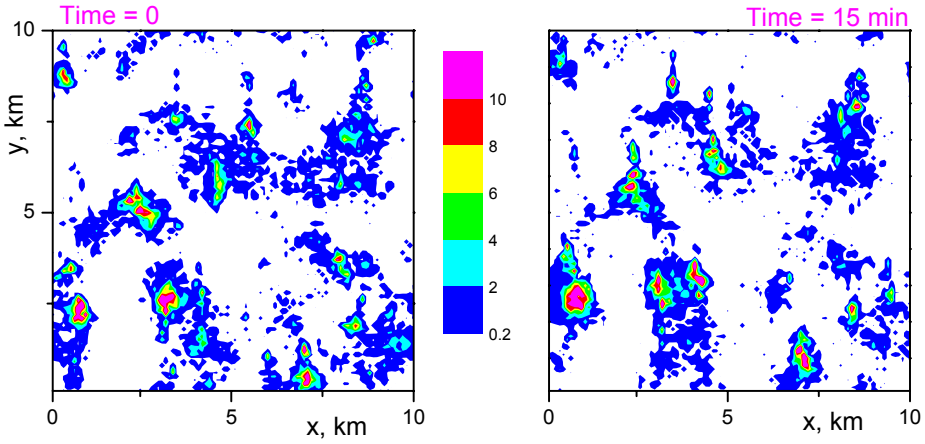

Figure 3. LES simulation. Horizontal distribution of cloud optical depth for different instants of time T; (a) T = 0, and (b) T = 15 min.

Results

We calculated $N_{nadir}(\alpha)$ and $N_{hemisph}(\alpha)$ for three different cross sections of cloud fields (in y-directions). Cross sections 1, 2, and 3 correspond to x = 1.6 km, x = 5 km and x = 8.6 km, respectively. These cross sections represent small, mean (close to domain-averaged) and large values of $N_{nadir}(0)$. Since the domain-averaged cloud fraction is almost time-independent (Figure 3), the time-averaged (15 min sample) properties $N_{nadir}(\alpha)$ and $N_{hemisph}(\alpha)$ are not sensitive to the cloud evolution (Figure 4). Therefore, hereafter we will consider results that are obtained for cloud field motion only. Note that $N_{nadir}(0)$, $N_{hemisph}(0)$ are equal and represent zenith-pointing ($\alpha = 0$) observations (such as a lidar or radar measurements). It is evident (Figure 4a) that $N_{nadir}(0)$ values (1) depend strongly on cross section and (2) can differ substantially from $N_{nadir,\ avr}$ ~0.28.

For example, $N_{nadir}(0)$ obtained for the cross section 3 is nearly twice as large as $N_{nadir,\ avr}$. It means, that the zenith pointing observations can significantly (more than 2 times) overestimate or, vice versa, underestimate the real cloud fraction for the domain ~10 x 10 km. In contrast, $N_{nadir}(80)$ values (1) depend weakly on cross section and (2) differ slightly from $N_{nadir,\ avr}$ (Figure 4a). Therefore, $N_{nadir}(80)$ can be representative for the large domain (~10 x 10 km). The question arises, how to derive $N_{nadir}(\alpha)$ from hemispherical observations (from $N_{hemisph}[\alpha]$)?

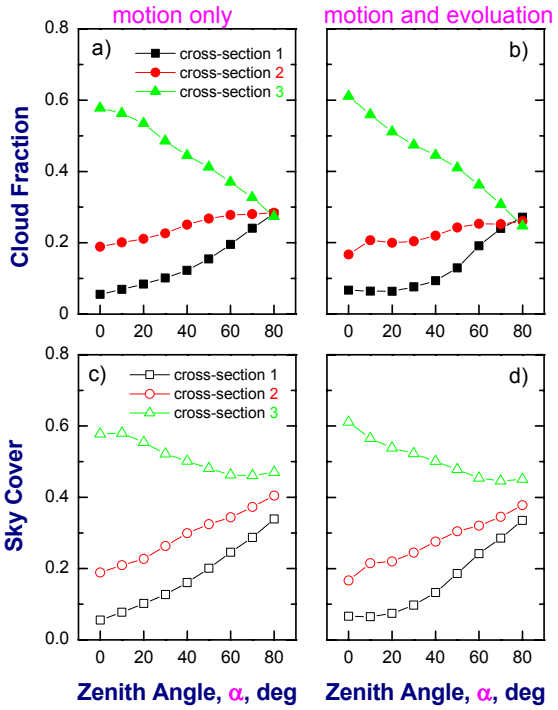

Figure 4. Nadir-view cloud fraction (a,b) and fractional sky cover (c,d) as functions of the cone zenith angle α, which are obtained for two sets of cloud fields generated by LES simulation: (a, c) first set (motion of cloud field only), (b,d) second set (motion and evolution of clouds).

From definitions of $N_{nadir}(\alpha)$ and $N_{hemisph}(\alpha)$ (Eqs. 1, 2) one can conclude that there are two main reasons for differences between these two functions. The first reason is the *observation conditions*: plane-parallel observations (from nadir) for $N_{nadir}(\alpha)$ and hemispherical ones (from surface) for $N_{hemisph}(\alpha)$. The second reason is *the vertical cloud size*: $N_{nadir}(\alpha)$ is independent of vertical cloud structure, in contrast, $N_{hemisph}(\alpha)$ can be sensitive to the vertical cloud variability. The latter can be explained as follows. For a fixed horizontal cloud distribution (e.g., for a given $N_{nadir}[\alpha]$), the probability of a clear line of sight is a monotonically decreasing function of zenith viewing angle, and the rate of decrease of this probability depends on the vertical cloud size stratification. Below we consider effect of the *observation conditions* and the *vertical cloud size* on the difference between $N_{nadir}(\alpha)$ and $N_{hemisph}(\alpha)$.

To estimate the effect of the *observation conditions* only, we perform Monte Carlo simulations assuming that the vertical cloud size is very small. We obtain the third additional set of 3D cloud fields from the first (original) set by reducing the vertical size of each pixel by factor of 100. As a result, the domain-averaged vertical cloud size, H, is very small (H ~0.001 km). In this case the differences between $N_{nadir}(\alpha)$ and $N_{hemisph}(\alpha)$ are due to the observation conditions (Figure 5a). There are substantial differences between $N_{nadir}(\alpha)$ and $N_{hemisph}(\alpha)$ for large α only (Figure 5a). Therefore, if the vertical cloud size is very small, then $N_{hemisph}(\alpha)$ can approximate $N_{nadir}(\alpha)$ quite accurately for $\alpha \leq 60$ (Figure 5a).

To estimate the combine effect of the both *observation conditions* and the *vertical cloud size*, we compare $N_{nadir}(\alpha)$ and $N_{hemisph}(\alpha)$ obtained for the first (original) set (see Approach section). The domain-averaged vertical cloud size is H ~0.1 km for this set. Therefore, the differences between $N_{nadir}(\alpha)$ and $N_{hemisph}(\alpha)$ are the result of both the observation conditions and the vertical cloud structure (Figure 5b). By comparing Figure 5a with Figure 5b, one can conclude the following: when the vertical cloud size extends, $N_{hemisph}(\alpha)$ increases and differences between $N_{nadir}(\alpha)$ and $N_{hemisph}(\alpha)$ can be magnified as well (Figure 5a, b).

The time-averaged (over 15 min sample) functions $N_{hemisph}(\alpha)$ and $N_{nadir}(\alpha)$ can be close to each other, but it does not mean that the same is true for their temporal realizations. For example, $N_{hemisph}(80)$ approximates $N_{nadir}(80)$ quite accurately for cross section 2 (Figure 5a). However, the temporal realizations of $N_{hemisph}(80)$ and $N_{nadir}(80)$ are very different (Figure 6): $N_{nadir}(80)$ is almost "flat", in contrast, $N_{hemisph}(80)$ shows clearly defined peak and valley. However, the averaging of highly sampled time series of $N_{hemisph}(\alpha)$ and $N_{nadir}(\alpha)$ allows one to decrease substantially the difference between time-averaged values of these two functions (Figure 5a).

Weak time-dependence of $N_{nadir}(80)$ can be explained as follows. For given cloud fields (Hb~0.7 km) and observation conditions (α = 80 degree), the radius of projection of the FOV onto the horizontal surface at height Hb, $R(\alpha)$, is about 4 km. Therefore, $N_{nadir}(80)$ is obtained for large area (~8 x 8 km) (Figure 7a, c) for each time step. These large areas (shifted in y-directions) have similar statistics. Obviously, $N_{nadir}(80)$ does not depend on location of individual clouds within these areas. Conversely, $N_{hemisph}(80)$ depends strongly on clouds positions within the FOV (Figure 7b, d). As a result, the peak in $N_{hemisph}(80)$ realization (Figure 6) is caused by clouds, which are located close to the center of the FOV (Figures 7b, d), while the valley (Figure 6) is due to clouds, which are observed close to the edge of FOV (Figures 7a, c).

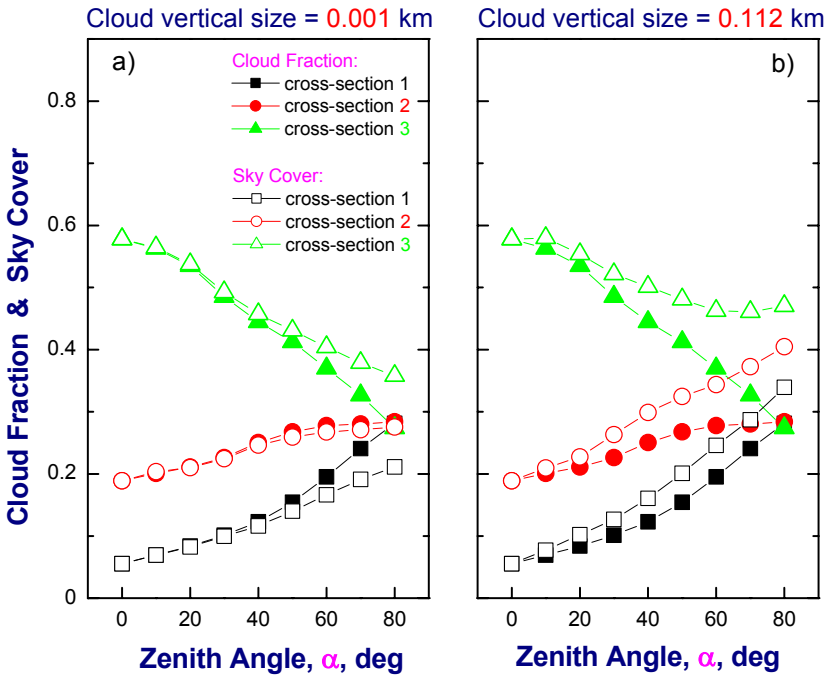

Figure 5. Nadir-view cloud fraction and fractional sky cover obtained for (b) the first set and (a) the third set of cloud fields produced by LES simulation. The only difference between these two sets is the vertical size of clouds. The mean vertical cloud size is 0.001km (the third set) and 0.112 km (the first set).

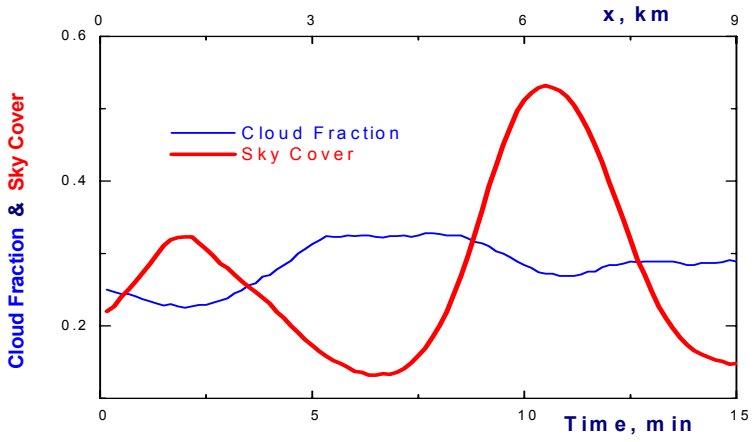

Figure 6. Temporal realizations of nadir-view cloud fraction and fractional sky cover for cross section 2 (x = 0.5 km), FOV with zenith angle 2α = 180 degree, and *H* ~0.001 km. A scale converting time to equivalent distance is given at the top of the figure.

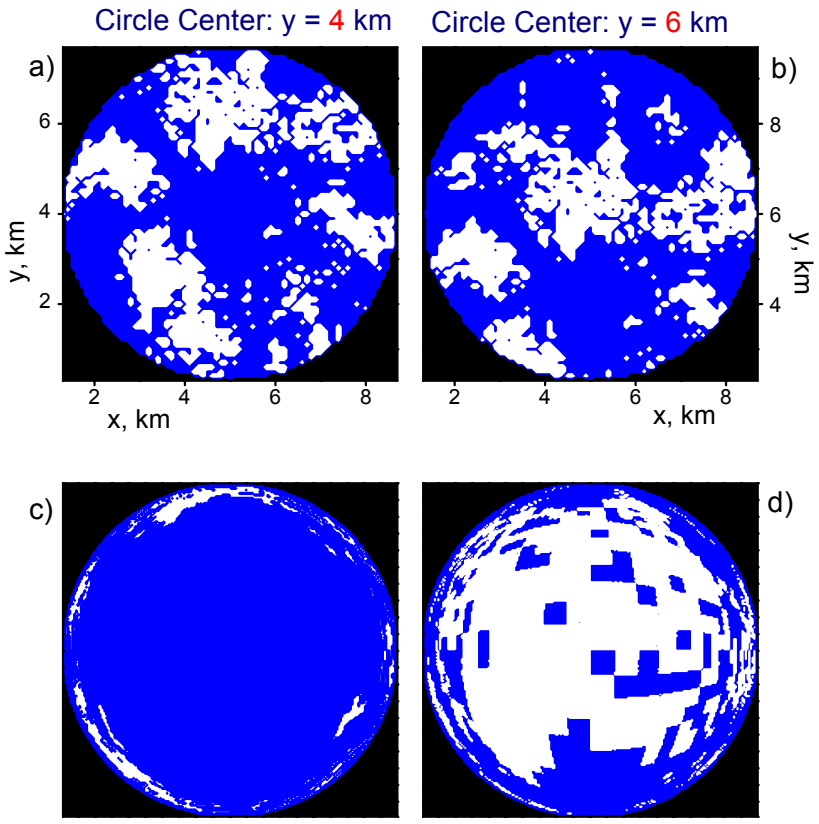

Figure 7. Images of nadir-view cloud fraction (a,b) and fractional sky cover (c,d) for the peak (b,d) and the valley (a,c) as shown in Figure 6. These images correspond to FOV with zenith angle 2α = 180° and cloud base height *Hb* = 0.66 km.

Weak time-dependence of $N_{nadir}(80)$ can be explained as follows. For given cloud fields (*Hb* ~0.7 km) and observation conditions (α = 80 degree), the radius of projection of the FOV onto the horizontal surface at height *Hb*, $R(\alpha)$, is about 4 km. Therefore, $N_{nadir}(80)$ is obtained for large area (~8 x 8 km) (Figures 7a, and c) for each time step. These large areas (shifted in y-directions) have similar statistics. Obviously, $N_{nadir}(80)$ does not depend on location of individual clouds within these areas. Conversely, $N_{hemisph}(80)$ depends strongly on clouds positions within the FOV (Figures 7b, and d). As a result, the peak in $N_{hemisph}(80)$ realization (Figure 6) is caused by clouds, which are located close to the center of the FOV (Figures 7b, and d), while the valley (Figure 6) is due to clouds, which are observed close to the edge of FOV (Figures 7a, and c).

Correction of Fractional Sky Cover

As noted above, the difference between $N_{nadir}(\alpha)$ and $N_{hemisph}(\alpha)$ are due to the *observation conditions* and the *vertical* distribution of clouds. Therefore, the approximate equation that links $N_{nadir}(\alpha)$ and

$N_{hemisph}(\alpha)$ should involve a parameter that specifies the *vertical cloud size*. Analysis of simulation results shows that relationship between $N_{nadir}(\alpha)$ and $N_{hemisph}(\alpha)$ can be described by:

$$N_{nadir}(\alpha) \sim N^{*}_{hemisph}(\alpha) \tag{8}$$

$$N^{*}_{hemisph}(\alpha) = N_{hemisph}(\alpha)\left(1 - \gamma(0)\frac{\alpha}{\alpha^{*}}\right) \tag{9}$$

where $\alpha^* = 80$, and $\gamma(0)$ is the cloud aspect ratio obtained from zenith-pointing observations ($\alpha = 0$); $\gamma(0) = H(0)/D(0)$, where $H(0)$ and $D(0)$ are the temporal mean of the vertical and horizontal cloud sizes, respectively. Recall that temporal averaging is performed over 15 min. sample. Here we use the mean value of cloud chord length as the mean horizontal cloud size $D(0)$. The cloud chord length is defined as the distance between the trailing and leading edges of a cloud for a given wind direction (in the y-direction). $N^*_{hemisph}(\alpha)$ can be considered as a *corrected* version of $N_{hemisph}(\alpha)$.

Let us discuss Eq. (9). First, we assume implicitly that $H(0)$ can be representative for the large area. Previously we have demonstrated that the mean vertical cloud size of small marine cumulus clouds depends weakly on both the spatial sample size and the sample cloud fraction (Kassianov et al. 2003). Conceivably this might be valid for other cloud types. Second, $N_{hemisph}(\alpha)$ is measured directly by TSI, and the cloud aspect ratio $\gamma(0)$ can be derived from collocated and coincident observations of zenith-pointing lidar/radar. Note that surface observations at ARM sites provide a means for such retrieval (e.g., Clothiaux et al. 1999, 2000). Third, Eq. (9) gives correct results for (1) completely overcast cloud field (in this case $D(0) >> H(0)$, and $\gamma(0) \sim 0$) and (2) clear-sky conditions.

The next example illustrates the application of Eq. (9). Values of $\gamma(0)$ obtained for three different cross sections (Table 1) are used to define the corresponding $N^*_{hemisph}(\alpha)$ functions (Figure 8). One can readily see that $N^*_{hemisph}(\alpha)$ matches $N_{nadir}(\alpha)$ closely for $\alpha \leq 60$ (Figures 8). This good agreement is attributed to the following two main reasons. First, $N_{hemisph}(\alpha)$ approximates $N_{nadir}(\alpha)$ reasonably well if $\alpha \leq 60$ and the mean vertical cloud size is negligibly small (e.g., Figure 5a). Second, $N^*_{hemisph}(\alpha)$ accounts for the mean vertical cloud size, $H(0)$, and $H(0)$ can be representative for the circle with radius $R(\alpha)$, where $\alpha \leq 60$. The large differences for cross section 1 and $\alpha > 60$ can be explained as follows. For cross section 1, the temporal mean value of $N_{nadir}(0)$ is very small (Figures 8a), therefore only a few cloud pixels have been used to estimate $H(0)$ and $D(0)$, and consequently, $\gamma(0)$. Certainly, these estimations ("poor" in statistical sense) are not representative for large areas (circles with radius $R(\alpha)$, where $\alpha > 60$). From Figure 8 we can conclude that the correction of fractional sky cover (see Eq. [9]) allows one to approximate the nadir-view cloud fraction quite accurately.

Table 1. The mean vertical, $H(0)$, horizontal, $D(0)$, size of clouds and corresponding cloud aspect ratio $\gamma(0)$ for three different cross sections and whole domain (10 x 10 km).

	Mean Vertical Cloud Size, km	Mean Horizontal Cloud Size, km	Cloud Aspect Ratio
Cross section 1	0.059	0.125	0.480
Cross section 2	0.085	0.425	0.200
Cross section 3	0.116	0.400	0.290
Domain-averaged	0.112	0.300	0.373

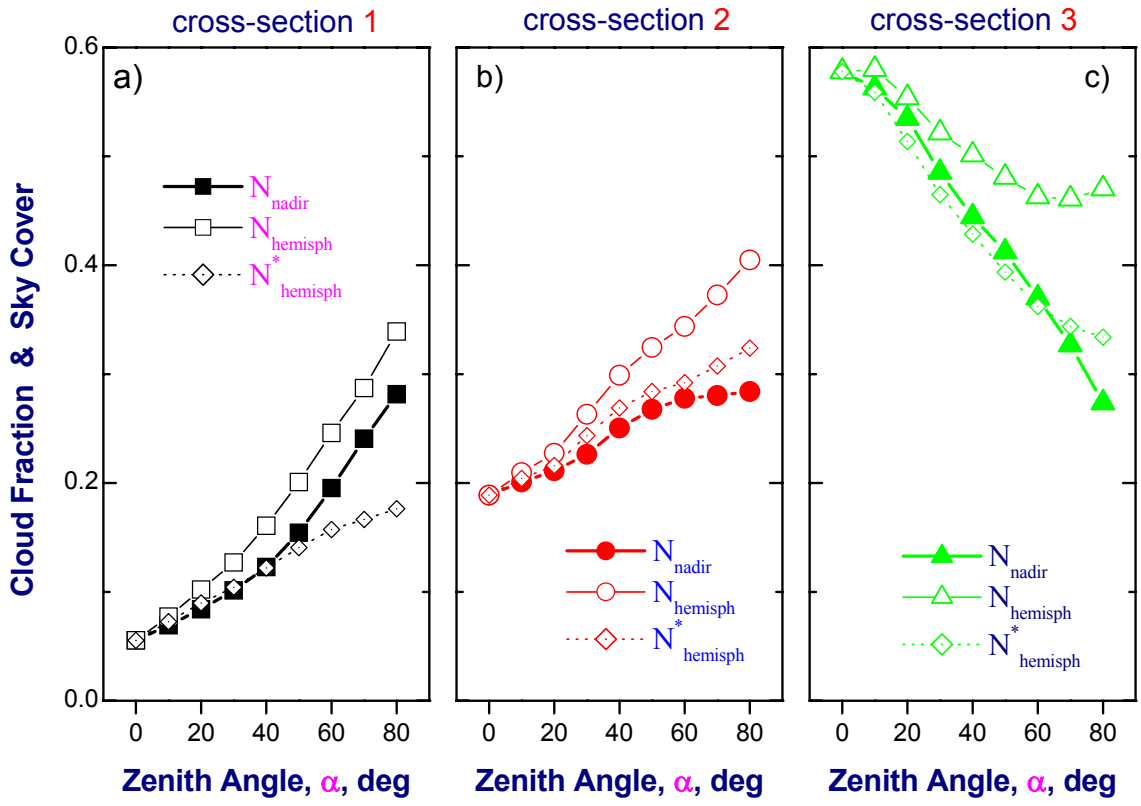

Figure 8. The nadir-view cloud fraction, $N_{nadir}(\alpha)$, fractional sky cover $N_{hemisph}(\alpha)$ and *corrected* fractional sky cover $N^*_{hemisph}(\alpha)$ obtained for different cross sections.

Conclusion

We considered the nadir-view cloud fraction, N_{nadir}, and the hemispherical fractional sky cover, $N_{hemisph}$, for different FOV with cone zenith angle 2α and estimate sensitivity of the time-averaged values of these bulk cloud statistics to the cloud evolution. For given cloud fields (generated by LES model), the effect of an individual cloud's evolution (local turbulence) on N_{nadir} and $N_{hemisph}$ is relatively small for a 15-min. temporal sample (the averaging period). This result is important, as it allows one to use only a single cloud realization for temporal simulations (Taylor's frozen flow hypothesis). These realizations can be obtained from satellite retrievals and/or stochastic simulations.

Also we demonstrate that contrary to N_{nadir}, instantaneous $N_{hemisph}$ is sensitive to the position of the clouds within the FOV and their vertical structure. However, an average from high temporal resolution samples of N_{nadir} and $N_{hemisph}$ greatly decreases this difference in the aggregate. The difference between N_{nadir} and $N_{hemisph}$ is a function of α. Finally we show that the angular dependence $N_{nadir}(\alpha)$ can be estimated quite accurately for $\alpha \leq 60$ if hemispherical observations of $N_{hemisph}(\alpha)$ are combined with information about the cloud aspect ratio. The latter could be derived from collocated and coincident zenith-pointing lidar/radar measurements or from a climatological database.

Because our comparison of $N^*_{hemisph}(\alpha)$ with $N_{nadir}(\alpha)$ is performed for a few cloud fields provided by LES model, further studies over additional cloud realizations/types are needed. Also we plan to verify this correction by using ground-based measurements (e.g., TSI, lidar/radar) and satellite (e.g., multi-angle imaging spectro radiometer) observations at ARM sites.

Acknowledgment

This work was supported by the Office of Biological and Environmental Research of the U.S. Department of Energy as part of the Atmospheric Radiation Measurement Program.

Corresponding Author

E. I. Kassianov, Evgueni.Kassianov@pnl.gov, (509) 372-6535

References

Clothiaux, E. E., K. P. Moran, B. E. Martner, T. P. Ackerman, G. G. Mace, T. Uttal, J. H. Mather, K. B. Widener, M. A. Miller, and D. J. Rodriguez, 1999: The Atmospheric Radiation Measurement Program cloud radars: Operational modes. *J. Atmos. Sci.,* **56**, 819-827.

Clothiaux, E., T. Ackerman, G. Mace, K. Moran, R. Marchand, M. Miller and B. Martner, 2000: Objective determination of cloud heights and radar reflectivities using a combination of active remote sensors at the ARM CART sites. *J. Appl. Meteorol*., **39**, 645-665.

Kassianov, E., T. Ackerman, R. Marchand, and M. Ovtchinnikov, 2003: Satellite multi-angle cumulus geometry retrieval: Case study. *J. Geophys. Res.*, (in press).